Published in final edited form as:
Cytometry A. 2010 November ; 77(11): 1020–1031. doi:10.1002/cyto.a.20970.

Tyramide signal amplification for analysis of kinase activity by intracellular flow cytometry

Matthew R. Clutter[1,2], **Garrett C. Heffner**[2], **Peter O. Krutzik**[1], **Kacey L. Sachen**[2], and **Garry P. Nolan**[1,*]

[1]Department of Microbiology and Immunology Baxter Laboratory for Stem Cell Biology Stanford University School of Medicine, Stanford, CA

[2]Program in Immunology Stanford University, Stanford, CA

Abstract

Intracellular flow cytometry permits quantitation of diverse molecular targets at the single-cell level. However, limitations in detection sensitivity inherently restrict the method, sometimes resulting in the inability to measure proteins of very low abundance or to differentiate cells expressing subtly different protein concentrations. To improve these measurements, an enzymatic amplification approach called tyramide signal amplification (TSA) was optimized for assessment of intracellular kinase cascades. First, Pacific Blue, Pacific Orange, and Alexa Fluor 488 tyramide reporters were shown to exhibit low non-specific binding in permeabilized cells. Next, the effects of antibody concentration, tyramide concentration, and reaction time on assay resolution were characterized. Use of optimized TSA resulted in a 10-fold or greater improvement in measurement resolution of endogenous Erk and Stat cell signaling pathways relative to standard, non-amplified detection. TSA also enhanced assay sensitivity and, in conjunction with fluorescent cell barcoding, improved assay performance according to a metric used to evaluate high-throughput drug screens. TSA was used to profile Stat1 phosphorylation in primary immune system cells, which revealed heterogeneity in various populations, including CD4+ FoxP3+ regulatory T cells. We anticipate the approach will be broadly applicable to intracellular flow cytometry assays with low signal-to-noise ratios.

Keywords

flow cytometry; intracellular flow cytometry; phospho flow; tyramide signal amplification; catalyzed reporter deposition; enzymatic amplification staining; cell signaling; signal transduction; cell-based assay; background

Introduction

Intracellular flow cytometry enables assessment of the relative concentrations of proteins in cultured or primary cells with single-cell resolution. Cells can be subjected to *in vivo* or exogenous manipulation, such as receptor-mediated stimulation or drug treatment, and subsequently fixed and permeabilized to preserve biochemical cell states and permit intracellular access to fluorescent detection antibodies (1–3). The technique allows rapid and simultaneous assessment of multiple steady-state and active-state proteins together with phenotypic markers in heterogeneous populations and rare cell subsets (4–8). Intracellular

*To whom correspondence should be addressed: Garry P. Nolan 269 Campus Dr. CCSR 3205 Stanford, CA 94305 Ph: 650-725-7002 Fax: 650-723-2383 gnolan@stanford.edu.

flow cytometry delivers highly quantitative measurements consistent with traditional biochemical methods (2,9,10).

Many intracellular molecules of interest, however, are expressed at low levels, perhaps at hundreds to only a few thousands of copies per cell. Detection of these targets using conventional flow cytometers and staining techniques is not reliable. Flow cytometric instrument detection limits in the fluorescein channel, for example, range from approximately 1000–3000 molecules (11,12). Cellular autofluorescence also plagues measurement sensitivity: one report determined that the 98th percentile of autofluorescence in various primary cell populations was equivalent to 2500–4000 fluorescein molecules (12). Therefore discriminating negative leukocytes from those bound with thousands of fluorescein-conjugated antibodies is often not possible. Detection can be performed in spectral regions with low cellular autofluorescence, but fluorophore choices are limited, collection optics and detection devices are never perfectly efficient, and one cannot completely escape background noise (13). In the end, it is not reasonable to expect that every endogenous target will be detectable by traditional flow cytometry. Accordingly, signal amplification approaches that improve detection sensitivity are needed.

Enhancement of flow cytometric sensitivity has been demonstrated using both multi-step indirect staining methods and enzyme-linked strategies (14,15). Although enzymatic approaches can theoretically amplify antibody detection by several orders of magnitude, application to flow cytometry was initially untenable because reporter chromophores or fluorophores washed away from cells. Catalyzed reporter deposition (CARD) involves enzyme-driven deposition and accumulation of a reporter molecule onto a surface (16). The technique was first applied to plate and membrane immunoassays and later extended to cell-based applications, including histochemistry, fluorescence and electron microscopy, and *in situ* hybridization (17–20). A common embodiment of CARD is tyramide signal amplification (TSA), which entails enzymatic deposition by horseradish peroxidase (HRP) of a tyramine-derivatized detection molecule, called a tyramide, in the presence of hydrogen peroxide. For cellular immunoassays, HRP molecules conjugated to cell-bound detection antibodies catalyze oxidation of tyramides into reactive free radicals that stably deposit onto local cellular macromolecules or oligomerize and precipitate in amounts proportional to target abundance (21,22). Successful application of TSA to flow cytometry was initially slow, but conditions were established that yield significant enhancement of cell surface marker measurements (23–25). Around the same time, Kaplan et al. and others applied the technique to achieve sensitive detection of intracellular proteins, including Epstein-Barr virus protein LMP-1, and human interferon-γ, interleukin-4, and D cyclins (25–27). Subsequently, measurement of D cyclins by TSA revealed differential expression in three B cell lymphoproliferative diseases (28). Recently, TSA-based measurement of intracellular signaling activity in leukemic B cells showed that basal levels of ZAP-70 and Syk phosphorylation were negatively correlated to total expression of ZAP-70 protein (29).

In light of the utility of TSA, this study aimed to quantitatively standardize the approach for intracellular flow cytometry by optimizing for superior measurement resolution of phospho-protein activation in intracellular kinase cascades. Cell signaling events afford readily "tunable" systems with broad, knowable ranges of relative target concentrations. Moreover, recent clinical focus on aberrant kinase activities in disease has prompted a general interest in application of intracellular flow cytometry for measurement of phospho-protein abundance. This technique, called phospho flow, has been used to discern endogenous kinase pathways in multiple human and mouse primary cell subsets, stratify patients, generate hypotheses regarding kinase dysregulation in cancer and autoimmunity, diagram signaling maps, and assess efficacy and pharmacodynamics of known drugs in patients and culture systems (5,6,9,30–39). Furthermore, drug screening in cell lines and primary cells

using phospho flow has allowed identification of compounds with activities specific to particular signaling pathways and cell subtypes (39–41).

We hypothesized that an optimized TSA approach would improve intracellular flow cytometry measurement resolution by overcoming instrument detection limits and cellular autofluorescence. A TSA protocol was empirically established that improved assay resolution and low-end sensitivity while maintaining a quantitative read-out of protein phosphorylation. TSA optimization first entailed screening a set of tyramides derivatized with different fluorescent molecules in permeabilized cells to identify reagents that demonstrated low non-specific binding. Pacific Blue, Pacific Orange, and Alexa Fluor 488 tyramides displayed low intracellular binding and exhibited robust deposition activities; for Pacific Blue and Pacific Orange, two relatively dim fluorophores, this meant that TSA facilitated intracellular detection in channels not ordinarily suited to measure scarce epitopes. Next, three critical variables were characterized within the TSA system—HRP-conjugated detection antibody concentration, tyramide concentration, and enzymatic reaction time—to test the effects of these variables on assay resolution. As determined by Z ′-factor, a commonly used means to evaluate the quality of high-throughput screens, amplification in conjunction with fluorescent cell barcoding (FCB) improved the overall performance of phospho flow assays (42). Finally, TSA was applied to profile Stat1 activation in mouse splenocyte populations in response to stimulation by multiple cytokines. Differential responses were observed across various immune cell populations such as CD4 T cells, regulatory T cells, and B cells. Intra-population heterogeneity was identified in response to multiple cytokines that was not detected by standard staining, suggesting broad utility of TSA in systems for detection of low abundance intracellular antigens.

Materials and Methods

Cell lines

U937 (human monocytic lymphoma) and Jurkat (human T cell leukemia) cells (ATCC, Manassas, VA) were maintained at 0.2×10^6–2×10^6 cells/mL in RPMI/10, composed of RPMI-1640 (Invitrogen, Carlsbad, CA) with 10% fetal bovine serum (Omega Scientific, Tarzana, CA), 100 U/mL penicillin, 100 μg/mL streptomycin, and 2 mM L-glutamine (Invitrogen).

Reagents

Phospho-specific Erk1/2 (T202/Y204; clone 197G2) was from Cell Signaling Technology (Danvers, MA). Phospho-specific Stat1 (Y701; clone 4a) conjugated to Alexa Fluor 488 was kindly provided by Becton Dickinson Pharmingen (San Jose, CA). Purified phospho-specific Stat1 (Y701; clone 4a) was kindly provided by BD Pharmingen and conjugated to Pacific Blue using an optimal ratio of Pacific Blue succinimidyl ester (Invitrogen) or to horseradish peroxidase (HRP) using maleimide-activated HRP (Sigma-Aldrich, St. Louis, MO) following antibody reduction with DL-dithiothreitol (DTT, Sigma-Aldrich). Goat-anti-rabbit-Alexa Fluor 488 (H+L), goat-anti-rabbit-Pacific Orange (H+L) and goat-anti-rabbit-HRP (ZyMAX™ grade) were from Invitrogen. Anti-mouse TCRβ-APC (clone H57-597), CD4-PerCP-Cy5.5 (clone RM4-5), and B220-Alexa Fluor 700 (clone RA3-6B2) were from BD Pharmingen. Anti-mouse FoxP3-PE (clone NRRF-30) was from eBioscience (San Diego, CA). Phorbol-12-myristate-13-acetate (PMA) was from EMD Biosciences (Merck KGaA, Darmstadt, Germany). Human recombinant interferon-γ (IFN-γ) and interleukin-6 (IL-6) were kindly provided by BD Pharmingen. Mouse recombinant granulocyte-macrophage colony-stimulating factor (GM-CSF), IFN-γ, IL-2, IL-3, IL-4, IL-6, IL-9, IL-10, and IL-13 were kindly provided by BD Pharmingen. Mouse recombinant IFN-α and IFN-β were from PBL InterferonSource (Piscataway, NJ). Mouse recombinant IL-21 was

from PeproTech (Rocky Hill, NJ). Bovine serum albumin (BSA), sodium azide, methanol, thimerosal, tyramine, N,N-dimethylformamide (DMF), triethylamine, dimethyl sulfoxide (DMSO), and ethanolamine were from Sigma-Aldrich. Hydrogen peroxide (30%, w/w) was from Thermo Fisher Scientific (Waltham, MA). Ampules of 16% paraformaldehyde in distilled water were from Electron Microscopy Sciences (Hatfield, PA).

Tyramide synthesis

Tyramide synthesis was adapted from Hopman et al. (43). Tyramine was dissolved in anhydrous DMF at 5 mg/mL. An equimolar amount of triethylamine was added to the tyramine solution. Fluorescent dyes and haptens were dissolved in DMF at 10 mg/mL and added to 1.1 equivalents of the tyramine solution. Succinimidyl esters of 6-(2,4-dinitrophenyl)aminohexanoic acid (DNP), Pacific Blue, Pacific Orange, 5-(and-6)-carboxyfluorescein (fluorescein), Alexa Fluor 488, Alexa Fluor 647, Alexa Fluor 680, Alexa Fluor 700, and Alexa Fluor 750 were from Invitrogen, the sulfo-succinimidyl ester of 6-(biotinamido)hexanoate (Biotin-LC) was from Thermo Fisher Scientific (Pierce Protein Research Products, Rockford, IL), and mono-reactive succinimidyl esters of Cy5 and Cy7 were from GE Healthcare (Piscataway, NJ). The reactions proceeded for 60 minutes at room temperature. To quench the reactions, ten equivalents of ethanolamine were added and reactions were allowed to stand for 20 minutes at room temperature. The reactions were then diluted with DMSO to 0.5–1 mg/mL with reference to the original dye amount for use in the TSA reaction.

Cell stimulation, staining, and amplification

Cells cultured to a density of approximately 10^6/mL were transferred to 5-mL round-bottom polystyrene tubes (Becton Dickinson Falcon) or 2-mL polypropylene 96-well microplates (VWR International, West Chester, PA) for stimulation at 37°C with PMA, IFN-γ, or IL-6 for 15 minutes. 10 nM PMA was used for maximal pErk induction, from which six consecutive two-fold dilutions were made to generate titration curve responses. 20 ng/mL IFN-γ and IL-6 were used for maximal pStat1 induction. Cells were then fixed with 1.5% PFA for 10 minutes at room temperature. After fixation, cells were pelleted at approximately 400 × g for 5 minutes, decanted, and resuspended in ice cold methanol for permeabilization. Cells were permeabilized at or below 4°C for at least 10 minutes. FCB was performed at this point, when applicable. Cells were then washed twice with sodium azide-free PBS containing 0.5% BSA (PBS/BSA) and resuspended in approximately 100 μL of PBS/BSA. Cells were stained with anti-pStat1 antibody conjugated to HRP, Alexa Fluor 488, or Pacific Blue, or with unlabeled pErk antibody for 30–60 minutes at room temperature or, in some cases, overnight at 4°C. Antibody concentrations are either listed in figures or optimal concentrations were used. After staining, cells were washed twice with PBS/BSA and aspirated nearly dry after the second wash. Standard phospho flow samples were resuspended in PBS containing 0.5% BSA and 0.02% sodium azide (PBS/BSA/NaN_3) prior to analysis. Amplified phospho flow samples were resuspended in amplification cocktail. The amplification cocktail consisted of tyramide and 0.003% H_2O_2 (approximately 1 mM) added to either commercial amplification buffer (Invitrogen, Tyramide Signal Amplification Kit, Component E) or an aqueous phosphate-buffered solution (10 mM sodium phosphate dibasic, 2 mM potassium phosphate monobasic, pH 7.4) containing 0.1% thimerosal. Tyramide concentrations and amplification times are described in the Results section. Addition of PBS/BSA/NaN_3 stopped the amplification reaction. Cells were washed with PBS/BSA/NaN_3 two to three times before data acquisition.

Mouse splenocyte isolation and phospho-Stat1 profiling

Splenocytes were obtained from 6–12 week old BALB/c female mice by glass slide homogenization and resuspended in RPMI/10 at 10^7 cells/ml. Cells were rested for

approximately 2 hours at 37° C prior to stimulation (6,34). All animal work was performed under approved Stanford APLAC/IACUC protocols. Splenocytes were stimulated with 100 ng/ml of the various cytokines for 15 minutes at 37°C. Cells were then fixed and permeabilized as described above. Unstimulated and stimulated cells were subjected to fluorescent cell barcoding and combined in a single tube prior to staining and amplification. Cells were stained with surface markers and 200 ng/ml anti-pStat1-HRP for 30 minutes at room temperature. Amplification was performed using 20 μM tyramide-Pacific Blue for 15 minutes.

Analysis of non-specific binding of tyramides and dyes

To measure non-specific binding properties of each of the tyramides and corresponding dyes, U937 cells were either untreated or fixed with 1.5% PFA at room temperature for 10 minutes, spun at 400 × g for 5 minutes, decanted, and resuspended in ice cold methanol for at least 10 minutes for permeabilization. Cells were washed twice with PBS/BSA/NaN_3 and resuspended in an aqueous phosphate-buffered solution (10 mM sodium phosphate dibasic, 2 mM potassium phosphate monobasic, pH 7.4, 0.1% thimerosal). Amine-reactive fluorescent dyes were pre-quenched with 10 molar equivalents of ethanolamine to yield non-reactive dyes. Tyramides and quenched dyes were added at the amounts specified and incubated at room temperature for 30 minutes. Cells were washed three times with PBS/BSA/NaN_3 prior to flow cytometry.

Fluorescent cell barcoding

Cells were subjected to FCB as previously described (41) using succinimidyl esters of Pacific Blue, Pacific Orange, Alexa Fluor 488, or Alexa Fluor 647 (Invitrogen). While cells were undergoing permeabilization in methanol they were incubated on ice for approximately 15 minutes with combinations of amine-reactive dyes. In some cases, dyes were added following permeabilization for 10 or more minutes, in which case methanol was diluted 1:3 with PBS. The cells were washed two times with PBS/BSA and combined together. Following acquisition, combined samples were deconvoluted during analysis. In most cases, stimulated cells were labeled with Alexa Fluor 647, washed, and combined with unlabeled, unstimulated cells prior to standard staining or TSA. The seven samples subjected to the PMA titration were all barcoded and combined using Alexa Fluor 488 and Alexa Fluor 647 prior to staining and acquisition, as were the sixteen samples (eight unstimulated and eight stimulated) used for Z′-factor calculations. For primary mouse splenocyte analysis, stimulated cells were labeled with Alexa Fluor 488 and combined with unstimulated, unlabeled cells.

Flow cytometry and data analysis

Flow cytometry was performed on a BD LSRII equipped with 405 nm, 488 nm, and 633 nm lasers. After acquisition, data was analyzed using FlowJo software (Tree Star, Ashland, OR). Median fluorescence intensity (MFI) values were determined for each population and phospho-protein fold change was calculated as $(MFI_{STIM})/(MFI_{UNSTIM})$. For Z′-factor calculations, mean MFI values (mean MFI) and standard deviations (SD) were calculated from unstimulated and stimulated replicate controls. Z′-factors were calculated as $1-((3\times SD_{UNSTIM}+3\times SD_{STIM})/(\text{mean } MFI_{STIM} - \text{mean } MFI_{UNSTIM}))$. Regression analysis and graphing were performed using Spotfire DecisionSite (TIBCO, Somerville, MA) or Microsoft Excel (Redmond, WA). Heat map visualization and hierarchical clustering with Ward's method were performed using Spotfire DecisionSite. For interdependency log-log summary plots, multiple anti-pStat1-HRP concentrations or reaction times were averaged to obtain the best value when multiple conditions yielded pStat1 fold change values within 20% of optimal.

Results

The TSA reaction schema and variables

The TSA approach used is outlined in Figure 1. Antibodies directed against intracellular epitopes, either directly conjugated to HRP or subsequently detected with HRP-labeled secondary antibody, bind targets in an amount proportional to target abundance. In the presence of hydrogen peroxide, HRP oxidizes fluorescent tyramide reporters to form short-lived free radical species that react with local cellular macromolecules or with one another. In either case, stable deposition of many fluorescent dyes is achieved in the vicinity of each protein target in an amount proportional to target abundance. Alternatively, hapten-labeled tyramide substrates may be used, followed by detection with a fluorescent anti-hapten reagent. To optimize TSA for detection of phosphorylated proteins by flow cytometry, problematic non-specific tyramide binding was first addressed by testing a set of diverse reagents in search of low background reporters. Three TSA critical amplification reaction variables were then characterized: detection antibody concentration, tyramide concentration, and enzymatic reaction time.

Tyramides with low non-specific intracellular binding

An obstacle common to intracellular staining techniques is high background signal generated by non-specific detection reagent binding (6,44). Initially, non-specific tyramide binding reduced the resolution of TSA assays and spectral overlap prohibited application of TSA to multiparametric flow cytometry. This was caused by the requirement that systems with high non-specific binding compensate with extremely high levels of reporter deposition, preventing detection in proximal measurement channels. Therefore, a variety of tyramide reagents were synthesized and their non-specific binding properties were characterized in permeabilized cells. Detection reagents were synthesized by conjugating tyramine to amine-reactive fluorescent dyes, specifically Pacific Blue, Pacific Orange, fluorescein, Alexa Fluor 488, Alexa Fluor 647, Alexa Fluor 680, Alexa Fluor 700, Alexa Fluor 750, Cy5, and Cy7.

Non-specific tyramide binding was first characterized in permeabilized cells across a range of concentrations (Figure 2A). The tyramides displayed vastly heterogeneous non-specific binding properties as indicated by the log ratio of the signal detected in the presence relative to the absence of tyramide. Cells incubated with 5 μM tyramide-Cy7 exhibited a signal nearly 3000 times higher than unstained cells (Figure 2B), whereas 5 μM Alexa Fluor 488 and Pacific Blue tyramides yielded signals approximately 10-fold above autofluorescence (Figures 2C and 2D, respectively). This indicates loss of assay resolution imparted by non-specific tyramide binding in a particular spectral region, but not necessarily the number of tyramide molecules binding to cells. Divergent intracellular binding behaviors perhaps reflected the molecular diversity of the tyramide structures. Figure 2E shows the log ratio calculations for tyramide-Cy7, tyramide-Alexa Fluor 488, and tyramide-Pacific Blue non-specific binding as reported in Figure 2A. Signals from Alexa Fluor 488 and Pacific Blue tyramide derivatives exceeded autofluorescence by less than one log at low concentrations and less than two logs at higher concentrations. TSA assays using Cy7, Cy5, Alexa Fluor 700, Alexa Fluor 680, and Alexa Fluor 750 tyramides, which yielded signals greater than two logs above autofluorescence at intermediate concentrations, did not improve measurement resolution relative to standard staining (data not shown).

To better understand the source of non-specific tyramide binding, the effects of cell permeabilization on tyramide background were tested (Supplemental Figure 1). In live cells, signals from nearly all tyramide reagents at 5 μM exceeded cellular autofluorescence by less than two logs. Upon permeabilization, non-specific binding signals increased for all

tyramides, generally by more than one log, although Pacific Orange, Pacific Blue, and Alexa Fluor 488 derivatives exhibited only 2–4 fold increases. To determine whether the fluorescent dyes mediated non-specific binding or if the tyramine group played a role, permeabilized cells were incubated with 5 μM tyramides or the corresponding fluorescent dyes. Approximately half of the fluorescent dyes displayed relatively low background binding, and the other half generated non-specific signals at least one log above cellular autofluorescence (Supplemental Figure 2). Signals in all channels increased approximately ten-fold when the tyramine group was present. These data underscore the need for careful selection of tyramides for intracellular TSA.

Optimizing key TSA variables

Tyramide-Pacific Blue was used to examine how critical variables affect TSA-based phospho-protein detection. This reagent was chosen because it displayed robust deposition and low non-specific intracellular binding. U937 cells were stimulated with IFN-γ or IL-6 to induce strong or weak Stat1 phosphorylation, respectively, to test if optimal assay parameters change for detection of small versus large biological signals relative to background. Preliminary data showed that TSA variables were interdependent (illustrated in Supplemental Figure 3), so the system was optimized by simultaneously permuting six concentrations of anti-pStat1-HRP, six concentrations of tyramide-Pacific Blue, and ten reaction times, for a total of 360 data points per stimulation. For each combinatorial assay condition, pStat1 fold change was calculated (MFI_{STIM} / MFI_{UNSTIM}) and plotted as a function of all discrete anti-pStat1-HRP concentrations (Figure 3A), tyramide-Pacific Blue concentrations (Figure 3B), or reaction times (Figure 3C) for IFN-γ (left panel, squares) or IL-6 (right panel, circles) stimulations.

A strong relationship was observed between anti-pStat1-HRP concentration and maximum pStat1 fold change (Figure 3A, blue lines). Anti-pStat1-HRP was optimal at 70 ng/mL for IFN-γ and IL-6 stimulation conditions and measurement resolution decreased 20–40% at three-fold higher and lower antibody concentrations. The sharp shape of these data indicated that anti-pStat1-HRP concentration was the most critical variable for successful application of TSA to intracellular flow cytometry.

The measured pStat1 fold change was also dependent on tyramide-Pacific Blue concentration. Higher concentrations yielded higher pStat1 resolution (Figure 3B). Optimal measurement of pStat1 induction by IFN-γ and IL-6 was obtained using 20 μM and 50 μM tyramide-Pacific Blue, respectively, although enhancement was not dramatically increased above 8 μM. The plateau-shaped data indicated that reaction-saturating concentrations of tyramide-Pacific Blue were optimal.

Finally, a 15 minute reaction was optimal for detecting strong pStat1 induction by IFN-γ and a 50 minute reaction was optimal for detecting weak pStat1 induction by IL-6 (Figure 3C). Favorable reaction times ranged from 1 to 30 minutes for IFN-γ and from 15 to 80 minutes for IL-6. Longer reaction times improved measurement sensitivity of weak phosphorylation induction, and shorter times yielded better resolution when measuring more abundant targets.

To compare TSA to standard staining methods, pStat1 was also measured using antibody directly conjugated to Alexa Fluor 488 (Figure 3D, top panels) or Pacific Blue (Figure 3D, middle panels). Pacific Blue is a relatively dim fluorescent dye with a lower quantum yield and extinction coefficient than Alexa Fluor 488. pStat1 induction was considerably weaker for IL-6 stimulation than for IFN-γ stimulation, and IL-6 induction was hardly discernable when directly conjugated Pacific Blue was used for detection (1.4-fold change). Detection of the same intracellular events using tyramide-Pacific Blue with optimized TSA yielded a 14–

30-fold improvement over directly conjugated Pacific Blue staining and a 10–13-fold improvement over directly conjugated Alexa Fluor 488 staining (Figure 3D, bottom panels). This demonstrated that amplification staining with a relatively dim fluorescent dye can be made effective with TSA and even improve upon direct staining with a brighter dye.

Interdependency of critical TSA variables

When optimizing for amplification, an appreciation that TSA variables are interdependent is important. If antibody concentration, tyramide concentration, or reaction time is held constant at a greatly suboptimal value, the variable being tested will compensate for it and fail to optimize correctly. Supplemental Figure 3 shows that each pair of the TSA variables presented in Figure 3 was inversely correlated. Optimal values of each variable were in turn held constant while data points spanning the other two variables were plotted (Supplemental Figure 3, left and center panels). Summary plots quantified the inverse relationships of each variable pair (Supplemental Figure 3, right panels). These data indicated that, when possible, the three variables should initially be titrated simultaneously to identify optimal or near-optimal conditions. However, small departures from optimal values of a variable are tolerable because additional variables can compensate.

Quantitative comparison of optimized TSA to standard methods

It was next determined how an optimized TSA approach compared to standard staining methods. Strong phosphorylation of Erk1/2 protein was induced in Jurkat cells by stimulation with 10 nM PMA and detected with Alexa Fluor 488 using either standard staining or TSA (Figure 4A, top and bottom panels respectively). TSA enhanced the measurement resolution of pErk1/2 in stimulated cells relative to unstimulated cells by approximately 10-fold versus standard phospho flow, yielding an extremely large fold change measurement (approximately 300-fold). This demonstrated that the optimization approaches outlined in Figure 3 were applicable to additional detection systems using tyramide reporters other than Pacific Blue. To test whether the technique improved low-end signal sensitivity in this system, weak Erk1/2 phosphorylation was induced in Jurkat cells with 0.3 nM PMA and detected with Pacific Blue dye using either standard staining or TSA (Figure 4B, top and bottom panels respectively). The amplification approach permitted resolution of pErk1/2 signal in stimulated cells relative to unstimulated cells (approximately 2-fold change), whereas standard staining did not differentiate the populations.

It was next assessed to what extent intracellular flow cytometry with TSA was quantitatively consistent with standard flow cytometry over a range of target protein concentrations. Treating Jurkat cells with a gradient of PMA concentrations induced a range of Erk1/2 phosphorylation states. The phospho-protein was detected with Pacific Orange dye using either standard flow cytometry methods or TSA (Figure 4C). TSA amplified the observed signals in proportion to standard phospho flow; low, intermediate, and high shifts relative to unstimulated cells were detected at increasing PMA concentrations using both techniques. The pErk1/2 fold change was plotted as a function of PMA concentration in Figure 4D. Standard and amplified staining approaches yielded PMA EC_{50} values of approximately 1 nM, but TSA afforded greater resolution of pErk1/2 fold change at nearly every PMA concentration. Amplification was useful at low PMA concentrations where little or no shift was detected by standard staining methods (Figure 4D, inset). Thus, TSA applied to intracellular flow cytometry provided a way to enhance signal resolution and low-end sensitivity with multiple fluorescent reporters while maintaining a readout that was quantitatively consistent with traditional flow cytometry.

TSA with fluorescent cell barcoding improved assay performance

Employing TSA to achieve better low-end sensitivity is advantageous in cases where amplification permits measurements that are undetectable by standard methods (e.g., Figure 4B and 4D). We hypothesized that the use of TSA to enhance measurements that are weakly detectable by standard phospho flow would improve the statistical robustness of such an assay. To address this question the TSA-based assay was compared to standard flow cytometry for multiple unstimulated and stimulated sample replicates. Fluorescent cell barcoding (FCB) was also evaluated in the context of TSA. FCB is a technique that dramatically increases throughput and staining consistency by enabling the combination of multiple samples into a single tube prior to antibody staining and amplification (41). Z′-factor, an established statistical metric of assay quality, was used for assay comparisons (42). Z′ values approach 1 as the separation between unstimulated and stimulated median fluorescence intensities (MFIs) increases to a value many times greater than the aggregate assay variance.

To test sample-to-sample variability, eight independent U937 cell replicates were unstimulated and eight replicates were stimulated with IL-6 to induce weak Stat1 phosphorylation. Cells were then either set aside or subjected to FCB. In each set of samples, levels of pStat1 induction were detected with Pacific Blue dye using either standard staining methods or TSA. TSA assays (Figure 5A, blue bars) displayed approximately a 10-fold enhancement in mean pStat1 fold change values relative to standard flow cytometry assays (Figure 5A, grey bars), which yielded approximately 1.4-fold pStat1 fold change. TSA without FCB yielded a wide range of possible pStat1 fold change values and had a lower Z′ (0.16) than either the non-FCB or FCB approaches under standard staining methods (0.68 and 0.63, respectively). This suggests that TSA magnified not only assay resolution but also variance. Use of FCB diminished TSA-based assay variance, probably because in FCB all sample replicates are stained and amplified in a single tube with identical enzymatic reaction conditions. TSA combined with FCB yielded a more reproducible assay ($Z' = 0.89$) than standard flow cytometry staining methods. MFI values of each of the eight unstimulated and stimulated controls were plotted for non-FCB and FCB assay conditions (Figure 5B). Replicates subjected to FCB displayed a narrower pStat1 distribution than replicates not subjected to FCB.

The benefit of FCB was also examined in a second system, in which pErk1/2 was detected in eight unstimulated and eight stimulated samples using TSA with tyramide-Pacific Blue (Figure 5C). Z′-factors of non-FCB (<0) and FCB (0.89) assays demonstrated that cell barcoding greatly improved assay quality. While TSA alone may increase assay variance relative to standard methods, amplification in the context of FCB yielded high-resolution, low-variance phospho-protein measurements. Phospho flow with TSA could become a useful tool in drug screening and compound profiling efforts.

Profiling Stat1 activation in primary mouse leukocytes using TSA

The effectiveness of TSA for phospho-protein detection was determined in mixed populations of differentially signaling primary cells. Mouse splenocytes were isolated, stimulated with a number of cytokines, and stained with surface markers for phenotyping. Stat1 phosphorylation was detected using standard staining or TSA. Lymphocytes responded differentially through Stat1 following IL-6 stimulation (Figure 6A). Nearly all T cells displayed strong Stat1 phosphorylation whereas few TCRβ-negative lymphocytes, primarily B cells, responded in this way. The effect was partially seen with standard staining, although it was not possible to accurately determine the frequency of responding T cells due to poor resolution of pStat1 in responders versus non-responders. For example, with standard staining 45% of T cells exhibited fluorescence intensity greater than the threshold set by the

TCRβ-negative population; with additional resolution provided by signal amplification, 93% of T cells responded at levels above the non-responding lymphocytes (Figure 6A, cells to the right of the vertical line). Note that TCRβ-APC survived the amplification protocol. A large set of fluorophores where examined to determined which survive the rigors of the TSA protocol. Most fluorescent reagents withstood the protocol, but some quantum dots, PE-Cy7, and Alexa Fluors 680, 700, and 750 lost greater than 25% of their original signal (data not shown). Therefore, in defined situations it will be optimal to use the latter agents to stain epitopes after performing TSA.

Since robust TSA detection of IL-6-induced Stat1 activation in a mixed lymphocyte population was informative, the analysis was extended to the five populations gated in Figure 6B: CD4 T cells (TCRβ+ CD4+), CD8 T cells (TCRβ+ CD4−), regulatory T cells (TCRβ+ CD4+ FoxP3+), B cells (B220+ TCRβ−), and a heterogeneous population composed primarily of monocytes and granulocytes (Forward Scatter-high). The populations were profiled for Stat1 activation in response to multiple cytokines, and the data were compiled into an immune cell Stat1 signaling fingerprint, displayed as a heat map (Figure 6C). Comparing TSA to standard staining, amplification yielded enhanced phospho-Stat1 detection, as indicated by a more brightly colored fingerprint. Taking advantage of the ability to quantify phospho-Stat1 induction by multiple cytokines across five cell populations at high resolution, hierarchical clustering was performed. This analysis provided an understanding of cytokine similarities with respect to Stat1 action in immune system cells. Interferon-α and interferon-β were closely related in this sense, and these two inflammatory factors were more closely related to IL-6 than to interferon-γ, which itself was most similar to IL-21. A number of cytokines that did not activate Stat1 in any cell type clustered together. Cell population clustering showed that the three T cell populations displayed very similar pStat1 responses, and that B cell responses were more similar to the mixed monocyte/granulocyte population than to any T cell population.

By improving phospho-Stat1 measurement resolution, TSA permitted identification of signaling not observable by standard staining and uncovered heterogeneity within primary cell populations (Figure 6D). Even in a population as refined as regulatory T cells, approximately 20% of cells failed to respond to IL-6 and only 10% of cells responded to IL-9. Regulatory T cells also exhibited a response to IL-21 and a broadly heterogeneous interferon-γ response. In addition, a subpopulation of B cells responded to IL-9 and a subpopulation of cells in the mixed Forward Scatter-high population responded to IL-6. Each of these observations was unpronounced with standard staining (Figure 6D, top panels). Overall these results support a broad utility of TSA for exploratory work characterizing signal transduction at the single cell level.

Discussion

Quantitative TSA detection of low abundance phospho-proteins, beyond the sensitivity range of many fluorophores, is here enabled for flow cytometry. Amplification improved assay resolution by up to 30-fold, enabled better measurement sensitivity than standard staining methods, and improved statistical assay performance in conjunction with FCB. The technique was applicable to cell lines and heterogeneous primary cell populations.

A number of publications have demonstrated expert use of TSA amplification and flow cytometry to quantify surface and intracellular protein levels in single cells (23–29). But to a novice the approach can be cumbersome due to the abundance of interdependent assay variables. The purpose of this study was to illustrate a standardized TSA approach where key variables were identified and their optimization was explored in depth. A detailed understanding of TSA variables will enable efficient adoption and advancement of the

technique. In addition, this study cataloged the utility of various tyramide reporters, including several previously unpublished reagents, as a resource to researchers performing high-parameter flow cytometry with amplification. Finally, these data demonstrate clear utility in highly heterogeneous primary cell populations.

Of biological interest, cytokine stimulation and downstream phosphorylated Stat1 measurement by TSA revealed functional heterogeneity within immune cell populations, which could lead to identification of novel cell types upon further characterization (Figure 6). For example, only 10% of splenic CD4+ FoxP3+ regulatory T cells responded to IL-9. Recently IL-9 was shown to enhance regulatory T cell suppressive functions in vitro, which raises the question of whether the effect is mediated solely by the small IL-9-responsive subpopulation (45). If so, the per cell suppressive potential of this subset is very high. In a second example, only a subset of B cells responded to IL-9 through pStat1. This subset could functionally correspond to human memory or germinal center B cells, both of which express IL-9α (46). In a prior study, IL-9 potentiated IgE production in germinal center B cells, suggesting that the subpopulation of IL-9-responsive B cells we observed could be involved in allergy or asthma initiation (46). These examples underscore the utility of TSA for single cell exploration of intracellular biochemistry.

In adopting TSA, tyramides with low non-specific intracellular binding were superior. Three tyramides with low binding were identified and used to enhance phospho flow measurements: Pacific Blue, Pacific Orange, and Alexa Fluor 488 (Figure 4). Tyramide-Alexa Fluor 647, tyramide-biotin, and tyramide-DNP were also used successfully (data not shown). Although tyramide-biotin and tyramide-DNP displayed low levels of non-specific binding, hapten-based TSA systems were difficult to optimize because staining of the fluorescent anti-hapten reagent must be performed at a saturating concentration to maintain quantitative accuracy. Overall, tyramides that generated more than 1–2 logs of non-specific signal over autofluorescence at 20 μM were not useful. The failure of such reagents was likely due in part to the high molecular weight of these tyramides, which probably diminished HRP active site accessibility and slowed diffusion. Although cell permeabilization and tyramine derivitization contributed to high non-specific tyramide binding, these are essential to the technique (Supplemental Figures 1 and 2). Pre-blocking cells with excess tyramine did not decrease non-specific tyramide binding, and washing with chaotropic agents, high salt buffers, or detergents only minimally improved assay resolution (data not shown). In the end, perhaps the best approach for dealing with non-specific binding is to identify additional low background reporters.

Optimization of TSA variables was important, and unlike standard flow cytometry staining, simultaneous titration of variables was required due to variable interdependency (Figure 3 and Supplemental Figure 3). Some general strategies for optimizing reaction variables are outlined in Supplemental Table 1. When HRP-labeled secondary staining is used with an unlabeled primary detection antibody, both antibodies should be titrated concurrently until an appropriate secondary concentration is established. Antibody concentration was a less forgiving variable than tyramide-Pacific Blue concentration and reaction time, each of which contained a plateau of acceptable values. Below-optimal detection antibody concentrations probably did not permit ample signal generation to overcome cellular autofluorescence and non-specific tyramide binding. Above-optimal concentrations probably resulted in high levels of non-specific antibody binding in negative control cells, leading to poor signal-to-noise. In our experience, these same antibody concentration effects are characteristic of non-amplified intracellular flow cytometry assays, whereas live cell staining resolution tends not to decline rapidly at high antibody concentrations. In general, antibody concentrations appropriate for TSA were lower than concentrations appropriate for standard staining. It was also determined that washing cells after antibody staining was more

important than in standard staining protocols. Whereas standard samples are traditionally washed once following antibody staining, TSA improved when samples were washed twice at this stage and at least twice following tyramide deposition.

Tyramide concentration was an important TSA variable and saturating concentrations provided optimal measurement resolution. 20 μM was appropriate for tyramide-Pacific Blue, but tyramides with different non-specific binding properties and deposition efficiencies can require different concentrations. Reaction time was another important TSA variable. Amplifying abundant targets required short reaction times (5–30 minutes) whereas long reaction times (20–120 minutes) better resolved weak phospho-protein induction. Reaction times from 5–60 minutes were sufficient for tyramide-Pacific Blue, but longer times can be optimal for substrates with less robust deposition.

A model was developed to better understand the effects of TSA assay variables on measurement resolution (Supplemental Figure 4). In flow cytometry, a measurement floor, established by instrument detection limits or cellular autofluorescence, becomes problematic when signals generated from specific antibody binding events do not significantly exceed this baseline – typically when autofluorescence is high or antigen abundance is low. For such cases, TSA increases the proportion of total signal derived from specific antibody binding events relative to autofluorescence. The model illustrates this by the convergence of theoretical and measured signal curves at some optimal reaction time (Supplemental Figure 4A, solid red region). Beyond this time, tyramide deposition site saturation or HRP inactivation form a measurement ceiling. Reaction conditions that control the rate of catalysis and deposition—tyramide concentration, fluorescent dye properties, hydrogen peroxide concentration, temperature, and reaction buffer composition—determine the times at which measured tyramide signals successively overcome background, approach theoretical resolution, and reach a ceiling. Thus, reaction time and tyramide concentration are key interdependent variables. These variables do not affect the theoretical assay resolution of a given biological system; that parameter is determined solely by detection antibody concentration. In summary, TSA generates signals that overcome background and approach theoretical limits determined by antibody binding ratios.

The model suggests two main ways to improve TSA. First, one can extend the time of signal accumulation prior to deposition site saturation or HRP inactivation. Theoretically, a system with prolonged fluorescent reporter deposition will yield a measured resolution closer to the true resolution of the biological system. Extending the time of productive deposition would especially benefit low abundance antigen detection because signal saturation probably occurs before tyramide deposition generates adequate signal-to-noise. For detection of abundant antigens, extending deposition time would improve assay resolution by permitting lower antibody concentrations. Pre-loading cells or antibodies with additional deposition sites (e.g., tyrosines), increasing tyramide free radical lifetimes with certain buffers, and engineering HRP to resist catalysis-mediated inactivation could each prolong productive tyramide deposition times. Second, one can eliminate the continuously increasing background signal that is generated by passive binding or deposition of tyramide in the absence of antibody-bound peroxidases. If such signal was eliminated, reactions proceeding for long times (hours to days) would yield optimal resolution, which would remove the requirement to stop catalysis at precise times. Preliminary data showed that quenching endogenous peroxidases was helpful for some cell types.

Using what was learned in this study, TSA was applied to intracellular staining of transcription factors and signaling proteins in rare mouse hematopoietic stem cell populations (Heffner, et al., manuscript in preparation). This application, together with Figure 6 data, demonstrated that an optimized protocol using low non-specific binding

tyramides could enable productive implementation of TSA in high-dimensional flow cytometry. Measurement of phospho-proteins with fluorescent dyes too weak for such evaluation by standard staining permitted the use of strong dyes for critical stem cell phenotypic measurements.

In summary, TSA for flow cytometry improved quantitative, single cell detection of endogenous intracellular antigens, and should be adopted for low abundance antigen detection and flow cytometry-based drug screening assays.

Supplementary Material

Refer to Web version on PubMed Central for supplementary material.

Acknowledgments

The authors thank Ken Schulz and Irv Weissman for helpful discussions.

Funding Support:

NHLBI N01-HV-28183

NIH U19 AI057229

Leukemia and Lymphoma Society 7017-6

NIH P01 CA034233-24

NIH HHSN272200700038C

NCI 1R01CA130826

References

1. Bauer KD, Jacobberger JW. Analysis of intracellular proteins. Methods Cell Biol. 1994; 41:351–76. [PubMed: 7532265]
2. Krutzik PO, Nolan GP. Intracellular phospho-protein staining techniques for flow cytometry: monitoring single cell signaling events. Cytometry A. 2003; 55A:61–70. [PubMed: 14505311]
3. Schulz KR, Danna EA, Krutzik PO, Nolan GP. Single-cell phospho-protein analysis by flow cytometry. Curr Protoc Immunol. 2007; Chapter 8(Unit 8):17. [PubMed: 18432997]
4. Lamoreaux L, Roederer M, Koup R. Intracellular cytokine optimization and standard operating procedure. Nat Protoc. 2006; 1:1507–16. [PubMed: 17406442]
5. Perez OD, Nolan GP. Simultaneous measurement of multiple active kinase states using polychromatic flow cytometry. Nat Biotechnol. 2002; 20:155–62. [PubMed: 11821861]
6. Krutzik PO, Clutter MR, Nolan GP. Coordinate analysis of murine immune cell surface markers and intracellular phosphoproteins by flow cytometry. J Immunol. 2005; 175:2357–65. [PubMed: 16081806]
7. Darzynkiewicz Z, Crissman H, Jacobberger JW. Cytometry of the cell cycle: cycling through history. Cytometry A. 2004; 58A:21–32. [PubMed: 14994216]
8. Krutzik PO, Irish JM, Nolan GP, Perez OD. Analysis of protein phosphorylation and cellular signaling events by flow cytometry: techniques and clinical applications. Clin Immunol. 2004; 110:206–21. [PubMed: 15047199]
9. Jacobberger JW, Sramkoski RM, Frisa PS, Ye PP, Gottlieb MA, Hedley DW, Shankey TV, Smith BL, Paniagua M, Goolsby CL. Immunoreactivity of Stat5 phosphorylated on tyrosine as a cell-based measure of Bcr/Abl kinase activity. Cytometry A. 2003; 54:75–88. [PubMed: 12879454]
10. Haas A, Weckbecker G, Welzenbach K. Intracellular Phospho-Flow cytometry reveals novel insights into TCR proximal signaling events. A comparison with Western blot. Cytometry A. 2008; 73A:799–807. [PubMed: 18548611]

11. Loken MR, Herzenberg LA. Analysis of cell populations with a fluorescence-activated cell sorter. Ann N Y Acad Sci. 1975; 254:163–71. [PubMed: 52308]
12. Schwartz A, Fernandez-Repollet E. Development of clinical standards for flow cytometry. Ann N Y Acad Sci. 1993; 677:28–39. [PubMed: 8388180]
13. Hoffman RA, Wood J. Characterization of Flow Cytometer Instrument Sensitivity. Curr Protoc Cytometry. 2007; Chapter 1(Unit 1):20.
14. Cohen JH, Aubry JP, Jouvin MH, Wijdenes J, Bancherau J, Kazatchkine M, Revillard JP. Enumeration of CR1 complement receptors on erythrocytes using a new method for detecting low density cell surface antigens by flow cytometry. J Immunol Methods. 1987; 99:53–8. [PubMed: 2952733]
15. Kim YR, Martin G, Paseltiner L, Ansley H, Ornstein L, Kanter RJ. Subtyping lymphocytes in peripheral blood by immunoperoxidase labeling and light scatter/absorption flow cytometry. Clin Chem. 1985; 31:1481–6. [PubMed: 3896568]
16. Bobrow MN, Harris TD, Shaughnessy KJ, Litt GJ. Catalyzed reporter deposition, a novel method of signal amplification. Application to immunoassays. J Immunol Methods. 1989; 125:279–85. [PubMed: 2558138]
17. Adams JC. Biotin amplification of biotin and horseradish peroxidase signals in histochemical stains. J Histochem Cytochem. 1992; 40:1457–63. [PubMed: 1527370]
18. Chao J, DeBiasio R, Zhu Z, Giuliano KA, Schmidt BF. Immunofluorescence signal amplification by the enzyme-catalyzed deposition of a fluorescent reporter substrate (CARD). Cytometry. 1996; 23:48–53. [PubMed: 14650440]
19. Mayer G, Bendayan M. Immunogold signal amplification: Application of the CARD approach to electron microscopy. J Histochem Cytochem. 1999; 47:421–30. [PubMed: 10082744]
20. Kerstens HM, Poddighe PJ, Hanselaar AG. A novel in situ hybridization signal amplification method based on the deposition of biotinylated tyramine. J Histochem Cytochem. 1995; 43:347–52. [PubMed: 7897179]
21. Gross AJ, Sizer IW. The oxidation of tyramine, tyrosine, and related compounds by peroxidase. J Biol Chem. 1959; 234:1611–4. [PubMed: 13654426]
22. Eling TE, Thompson DC, Foureman GL, Curtis JF, Hughes MF. Prostaglandin H synthase and xenobiotic oxidation. Annu Rev Pharmacol Toxicol. 1990; 30:1–45. [PubMed: 2111654]
23. Kaplan D, Smith D. Enzymatic amplification staining for flow cytometric analysis of cell surface molecules. Cytometry. 2000; 40:81–5. [PubMed: 10754521]
24. Kaplan D, Meyerson H, Lewandowska K. High resolution immunophenotypic analysis of chronic lymphocytic leukemic cells by enzymatic amplification staining. Am J Clin Pathol. 2001; 116:429–36. [PubMed: 11554172]
25. Kaplan D, Smith D, Meyerson H, Pecora N, Lewandowska K. CD5 expression by B lymphocytes and its regulation upon Epstein-Barr virus transformation. Proc Natl Acad Sci U S A. 2001; 98:13850–3. [PubMed: 11707593]
26. Karkmann U, Radbruch A, Holzel V, Scheffold A. Enzymatic signal amplification for sensitive detection of intracellular antigens by flow cytometry. J Immunol Methods. 1999; 230:113–20. [PubMed: 10594358]
27. Kaplan D, Meyerson H, Husel W, Lewandowska K, MacLennan G. D cyclins in lymphocytes. Cytometry A. 2005; 63A:1–9. [PubMed: 15619730]
28. Meyerson HJ, MacLennan G, Husel W, Cocco A, Tse W, Lazarus HM, Kaplan D. D cyclins in CD5+ B-cell lymphoproliferative disorders: cyclin D1 and cyclin D2 identify diagnostic groups and cyclin D1 correlates with ZAP-70 expression in chronic lymphocytic leukemia. Am J Clin Pathol. 2006; 125:241–50. [PubMed: 16393687]
29. Kaplan D, Meyerson HJ, Li X, Drasny C, Liu F, Costaldi M, Barr P, Lazarus HM. Correlation between ZAP-70, phospho-ZAP-70, and phospho-Syk expression in leukemic cells from patients with CLL. Cytometry B Clin Cytom. 2010; 78B:115–22. [PubMed: 20014315]
30. Zell T, Khoruts A, Ingulli E, Bonnevier JL, Mueller DL, Jenkins MK. Single-cell analysis of signal transduction in CD4 T cells stimulated by antigen in vivo. Proc Natl Acad Sci U S A. 2001; 98:10805–10. [PubMed: 11535838]

31. Chow S, Patel H, Hedley DW. Measurement of MAP kinase activation by flow cytometry using phospho-specific antibodies to MEK and ERK: potential for pharmacodynamic monitoring of signal transduction inhibitors. Cytometry. 2001; 46:72–8. [PubMed: 11309815]
32. Ilangumaran S, Finan D, Rottapel R. Flow cytometric analysis of cytokine receptor signal transduction. J Immunol Methods. 2003; 278:221–34. [PubMed: 12957410]
33. Irish JM, Hovland R, Krutzik PO, Perez OD, Bruserud O, Gjertsen BT, Nolan GP. Single cell profiling of potentiated phospho-protein networks in cancer cells. Cell. 2004; 118:217–28. [PubMed: 15260991]
34. Krutzik PO, Hale MB, Nolan GP. Characterization of the murine immunological signaling network with phosphospecific flow cytometry. J Immunol. 2005; 175:2366–73. [PubMed: 16081807]
35. Sachs K, Perez O, Pe'er D, Lauffenburger DA, Nolan GP. Causal protein-signaling networks derived from multiparameter single-cell data. Science. 2005; 308:523–9. [PubMed: 15845847]
36. Irish JM, Czerwinski DK, Nolan GP, Levy R. Kinetics of B cell receptor signaling in human B cell subsets mapped by phosphospecific flow cytometry. J Immunol. 2006; 177:1581–9. [PubMed: 16849466]
37. Danna EA, Nolan GP. Transcending the biomarker mindset: deciphering disease mechanisms at the single cell level. Curr Opin Chem Biol. 2006; 10:20–7. [PubMed: 16406766]
38. Hale MB, Nolan GP. Phospho-specific flow cytometry: intersection of immunology and biochemistry at the single-cell level. Curr Opin Mol Ther. 2006; 8:215–24. [PubMed: 16774041]
39. Krutzik PO, Crane JM, Clutter MR, Nolan GP. High-content single-cell drug screening with phosphospecific flow cytometry. Nat Chem Biol. 2008; 4:132–42. [PubMed: 18157122]
40. Clutter MR, Krutzik PO, Nolan GP. Phospho-specific flow cytometry in drug discovery. Drug Discovery Today: Technologies. 2005; 2:295–302.
41. Krutzik PO, Nolan GP. Fluorescent cell barcoding in flow cytometry allows high-throughput drug screening and signaling profiling. Nat Methods. 2006; 3:361–8. [PubMed: 16628206]
42. Zhang JH, Chung TD, Oldenburg KR. A Simple Statistical Parameter for Use in Evaluation and Validation of High Throughput Screening Assays. J Biomol Screen. 1999; 4:67–73. [PubMed: 10838414]
43. Hopman AH, Ramaekers FC, Speel EJ. Rapid synthesis of biotin-, digoxigenin-, trinitrophenyl-, and fluorochrome-labeled tyramides and their application for In situ hybridization using CARD amplification. J Histochem Cytochem. 1998; 46:771–7. [PubMed: 9603790]
44. Hulspas R, O'Gorman MR, Wood BL, Gratama JW, Sutherland DR. Considerations for the control of background fluorescence in clinical flow cytometry. Cytometry B Clin Cytom. 2009; 76B:355–64. [PubMed: 19575390]
45. Elyaman W, Bradshaw EM, Uyttenhove C, Dardalhon V, Awasthi A, Imitola J, Bettelli E, Oukka M, van Snick J, Renauld JC, et al. IL-9 induces differentiation of TH17 cells and enhances function of FoxP3+ natural regulatory T cells. Proc Natl Acad Sci U S A. 2009; 106:12885–90. [PubMed: 19433802]
46. Fawaz LM, Sharif-Askari E, Hajoui O, Soussi-Gounni A, Hamid Q, Mazer BD. Expression of IL-9 receptor alpha chain on human germinal center B cells modulates IgE secretion. J Allergy Clin Immunol. 2007; 120:1208–15. [PubMed: 17919707]

Figure 1.
The TSA reaction and important variables. Antibodies labeled with HRP are used to detect specific intracellular targets like phospho-proteins in permeabilized cells. Alternatively, unlabeled antibodies are used in combination with secondary HRP-labeled antibodies. The concentration of HRP in a cell is thus proportional to target abundance. Tyramine, an HRP substrate, is covalently appended to a fluorescent dye suitable for flow cytometric detection to create a tyramide. In the presence of hydrogen peroxide, HRP oxidizes tyramide to form reactive free radicals that stably deposit onto local cellular macromolecules or that react with one another to form oligomeric precipitate. Over time, tyramides continuously deposit within a cell, which amplifies the fluorescent signal relative to what is achieved by standard staining methods. The reaction variables boxed in red were critical for TSA application to intracellular flow cytometry.

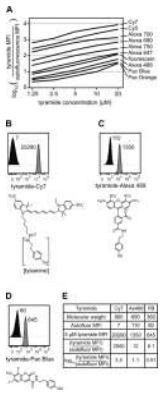

Figure 2.

Fluorescent tyramides displayed diverse non-specific intracellular binding. (A) U937 cells were fixed, permeabilized, and incubated with different tyramide reporters at various concentrations. Non-specific tyramide binding was calculated relative to autofluorescence as $\log_{10}$((tyramide MFI)/(autofluorescence MFI)). (B) U937 cells were fixed, permeabilized, and incubated with or without 5 μM tyramide-Cy7 for 30 minutes in the absence of exogenous peroxidase and hydrogen peroxide. MFI values measured by flow cytometry for the tyramide (grey histogram) and for autofluorescence in the corresponding channel (black histogram) are reported. The structure of tyramide-Cy7 is below the plot with the tyramine portion in brackets. (C) Non-specific intracellular binding by 5 μM tyramide-Alexa Fluor 488 was assessed as in (B). (D) Non-specific intracellular binding by 5 μM tyramide-Pacific Blue was assessed as in (B). (E) Summary for Cy7, Alexa Fluor 488, and Pacific Blue tyramides demonstrating calculation of the non-specific binding metric reported in (A).

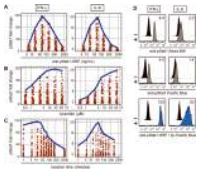

Figure 3.

Antibody concentration, tyramide concentration, and reaction time were important TSA variables. (A) U937 cells were either unstimulated or stimulated with IFN-γ (left panel, square markers) or IL-6 (right panel, circle markers) and subjected to TSA under 360 different reaction conditions derived from concurrent titration of six anti-pStat1-HRP concentrations, six tyramide-Pacific Blue concentrations, and ten reaction times. pStat1 fold change values (MFI_{STIM} / MFI_{UNSTIM}) were plotted for different assay conditions at each discrete anti-pStat1-HRP concentration. The bold blue line indicates maximum assay resolution at a given anti-pStat1-HRP concentration. (B) Tyramide-Pacific Blue concentration was explored in a manner similar to anti-pStat1-HRP concentration in (A). (C) Reaction time was explored in a manner similar to anti-pStat1-HRP concentration in (A). (D) U937 cells were either unstimulated or stimulated with IFN-γ (left panels) or IL-6 (right panels) and stained with anti-pStat1 antibody conjugated to Alexa Fluor 488 (top panels), Pacific Blue (middle panels), or HRP (bottom panels). HRP-labeled cells were subjected to TSA under optimal conditions (IFN-γ: 70 ng/mL anti-pStat1-HRP, 20 μM tyramide-Pacific Blue, 15 minutes; IL-6: 70 ng/mL anti-pStat1-HRP, 50 μM tyramide-Pacific Blue, 50 minutes). MFIs of unstimulated (black histograms) and stimulated (grey and blue histograms) cells were used to calculate the pStat1 fold change values reported in each plot.

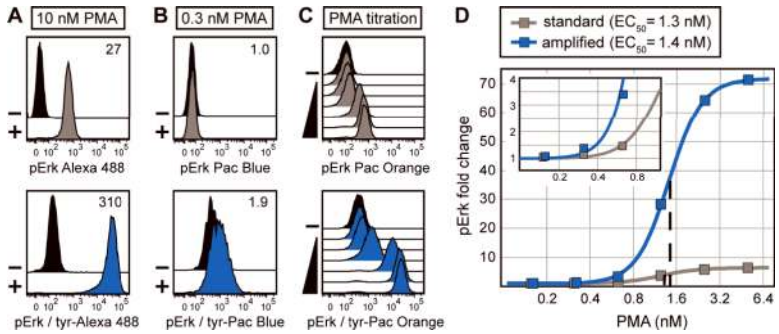

Figure 4.

TSA is quantitative and has higher sensitivity than standard methods. (A) Jurkat cells were unstimulated (black histograms) or stimulated with 10 nM PMA to induce maximal Erk1/2 phosphorylation. pErk1/2 levels were detected with an unlabeled primary antibody followed by a secondary antibody labeled with either Alexa Fluor 488 (grey histogram) or HRP (blue histogram). HRP-stained cells were subjected to TSA with 20 μM tyramide-Alexa Fluor 488 for 60 minutes. pErk1/2 fold change values (MFI_{STIM} / MFI_{UNSTIM}) are reported in each plot. (B) Jurkat cells were stimulated with 0.3 nM PMA and low levels of pErk1/2 were detected and displayed as in (A). Amplification was performed with 8 μM tyramide-Pacific Blue for 10 minutes. (C) Jurkat cells were unstimulated or stimulated with various concentrations of PMA (from 0.15 μM to 10 μM) and levels of pErk1/2 were detected and displayed as in (A). Amplification was performed with 30 μM tyramide-Pacific Orange for 20 minutes. (D) pErk1/2 fold change values were calculated at each point in the PMA titration from (C) and plotted as a function of PMA concentration. PMA EC_{50} values were determined by logistic regression analysis for standard staining (grey curve, 1.3 nM) and TSA (blue curve, 1.4 nM). The inset shows data at low PMA concentrations.

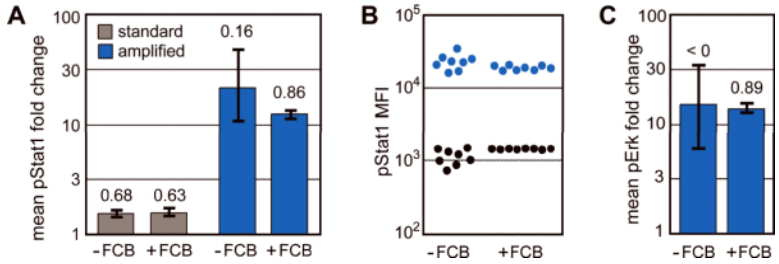

Figure 5.

Fluorescent cell barcoding (FCB) improves TSA assays. (A) Eight independent replicates of both unstimulated and IL-6 stimulated U937 cell samples were split for either individual sample processing or FCB. For FCB, the 16 replicates were labeled with unique fluorescent signatures and combined. The samples were then subjected to staining and flow cytometry to detect pStat1 with Pacific Blue dye using either standard methods or TSA (30 μM tyramide for 45 minutes). Mean pStat1 fold change values (mean MFI_{STIM} / mean MFI_{UNSTIM}) were calculated for standard staining (grey bars) and TSA (blue bars). For each assay the range of pStat1 fold change values (eight stimulated samples each compared to eight unstimulated samples) is marked with a black range bar. Z′-factors are reported above the bars. Higher Z′ values correspond to better assay reproducibility. (B) pStat1 MFI values of the eight unstimulated (black) and eight stimulated (blue) samples subjected to TSA as described in (A) were plotted. The data are spread horizontally to show sample variance. (C) Eight independent replicates of both unstimulated and PMA stimulated U937 cells were split for either individual sample processing or FCB. Samples were stained with pErk1/2 detection antibody followed by HRP-labeled secondary antibody and were subjected to TSA (20 μM tyramide-Pacific Blue for 10 minutes). Fold change ranges and Z′-factors are displayed as described in (A).

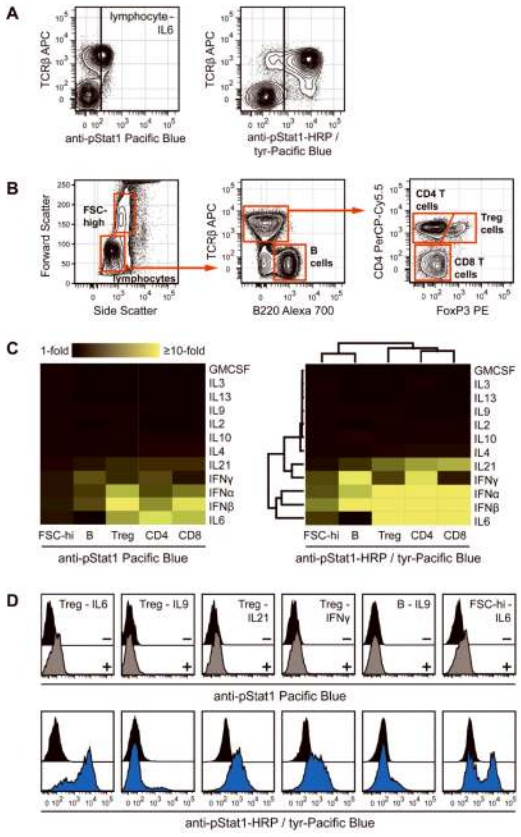

Figure 6.

Stat1 activation profiling in primary mouse splenocytes. (A) Splenocytes were stimulated with IL-6 and stained with TCRβ antibody to identify T cells. Standard staining (left panel) or TSA (right panel) were used to measure Stat1 phosphorylation. TCRβ-negative non-responding cell populations determined the black vertical activation bounds in each plot. (B) Gating strategy for mouse splenocyte populations. A high forward scatter population (composed primarily of monocytes and granulocytes) and a low forward scatter population (lymphocytes) were gated first. Within the lymphocytes, TCRβ+ B220− T cells and B220+ TCRβ− B cells were gated. Within T cells, CD4− FoxP3− cells (CD8 T cells), CD4+ FoxP3− cells (CD4 T cells), and CD4+ FoxP3+ cells (regulatory T cells) were identified. (C) Splenocytes were stimulated with the cytokines listed alongside the heat maps and standard staining (left panel) or TSA (right panel) were used to measure Stat1 activation in the five cell populations from (B). TSA-based pStat1 measurements were used for hierarchical clustering to understand the relatedness of cytokines and cell populations to one another. (D) Certain data from the pStat1 fingerprint are displayed to show that TSA (bottom row, blue histograms) but not standard staining (top row, grey histograms) identified underlying heterogeneity within cell populations. Black histograms were unstimulated cells.